Advances in Applied Mathematics and Mechanics
Adv. Appl. Math. Mech., Vol. **5**, No. 5, pp. 671-687

DOI: 10.4208/aamm.12-m1250
October 2013

Kinematics and Mechanical Properties Analyses on Vibration Converter of Intelligent Damper for Drill Strings

Xiaohua Zhu* and Chunlin Lai

College of Mechatronic Engineering, Southwest Petroleum University, Chengdu 610500, Sichuan, China

Received 10 April 2012; Accepted (in revised version) 19 March 2013

Available online 31 July 2013

Abstract. Taking vibration converter of intelligent damper for drill strings as the study object, this paper analyzes the influential factors of motion state of the ball and conducts an explicit dynamics simulation by establishing a mechanics model of vibration converter. The study basis is Newton's laws of motion, d'alembert's principle and hertz contact theory. And we use world coordinate system, rotating coordinate system and Frenet coordinate system to deduce kinematics equations of vibration converter.The ultimate result demonstrates that the axial velocity and maximum contact stress change with the increment of ball diameter and helix angle.It also proves the validity of our derived kinematics and mechanical models and provides a good consultant value for the design and theoretical arithmetic of vibration converter for intelligent damper of drill strings.

AMS subject classifications: 51N20, 53A17, 74A10, 74S05

Key words: Intelligent damper, vibration, converter, kinematics analysis, contact stress.

1 Introduction

As a rotating slender elastic rod, drill strings works under complex conditions. Rock breaking excitation and borehole constraint during its work exerts axial vibration, lateral vibration and torsional vibration on drill strings (Fig. 1), especially in hard formation or soft-hard interlayer. These vibrations can cause serious damages on well-drilling. From variations in weight on bit (WOB) and drilling torque, premature failure of bit, aggravated fatigue of drill strings, thread gluing and fracture, to ground equipment damage, these damages will lead to failure of the valued downhole tools (MWD, LWD and RSS [1]), overall time rises and huge losses. Therefore, vibration mitigation is greatly

*Corresponding author.
Email: zxhth113@163.com (X. H. Zhu)

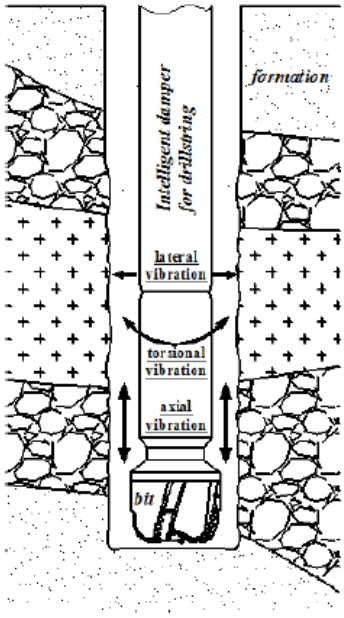

Figure 1: Bottom hole assembly (BHA) and vibration modes.

needed and drill strings damper is a most effective way. In this field, intelligent dampers represent the latest tendency of downhole vibration damping techniques [2], which can monitor real-time drill strings vibration and attenuate it.

The common spring dampers are only able to buffer or eliminate axial vibration. The air damper, with pressurized inert gas injected into the seal cavity, works well in absorbing vibrations by changing its cavity volume. However, the complexity of seal structure is a fatal weakness, and the preseted pressure of inert gas also limits its damping capacity [3]. Overcoming all the drawbacks above is the intelligent damper for drill strings, which can eliminate both axial vibration and torsional vibration simultaneously, as well as providing a wide damping range and long service life.

Vibration converter, as a key part of the intelligent damper for drill strings, take the function of converting torsional vibration into axial vibration. This converted axial vibration, adding up with original axial vibration is mitigated simply by the axial damping elements. To realize that torsional-axial convert, vibration converter usually adopts ball screw. Ball works as an intermediary for transmitting motion and force as well as transforming rolling friction into sliding friction. Therefore, its motion and stress situation has direct effects on the motion characteristics of vibration converter. In the general mechanical industry, the motion characteristics and mechanical properties of ball have been much investigated. D. Mundo and H. S. Yan proposed a method for the kinematics optimization of ball screw transmission mechanisms [4], Yoshida Takafumi et al. presented an analytical method which can be used to determine the motion of the ball and the ball load distribution, and then a parametric study on a ball screw was carried out to esti-

mate the effectiveness of the method as a design tool [5]. Xuesong Mei et al. developed a model to analyze the load distribution of ball screws with geometry errors, and made the opinion that the positive geometry errors of the ball screw result in the increase of the load on balls or guiding grooves [6]. Xian-Chun Song, Hong-Kui Jiang et al. analyzed the elastic deformation of high speed ball screw based on the finite element method [7]. These studies pay their attention mainly on the ball screw between the helix angle of $3^\circ \sim 17^\circ$, but the vibration converter of intelligent damper for drill strings needs a wider helix angle for its physical dimension restriction. So far, studies on wider range of helix angle have not been found among published literatures. As the kinematics and mechanical properties changing with the increase of helix angle, it is essential to investigate the properties of ball screw at wider helix angle to provide instructions for the design of vibration converter of intelligent damper for drill strings and improvements on the existing theory of ball screw.

From kinematics aspect, this paper establishes kinematics model for vibration converter to make theoretically calculations and analysis of kinematics characteristics of the ball. Besides, we also analyze contact in the vibration converter and set up the expressions for contact stress and strain. At last, the final explicit dynamics simulation on the vibration converter is done by SolidWorks and ABAQUS.

2 Vibration converter model

The designed intelligent damper for drill strings is shown in Fig. 2, and the vibration converter presented in this paper is part of it. The intelligent damper for drill strings is coupled to drill strings near bit. The drilling fluid drives the turbine generator to power the sensor, controller, and MR fluid damper during the work. Meanwhile, the sensor measures the vibration and provides this information to the controller in the form of electrical current via which the controller can control the magnitude of the electrical current to vary the strength of the aggregate magnetic field, and thus adjust the damping of the MR fluid. Under normal conditions, MR fluid has the flow characteristics of conventional oil. In the presence of a magnetic field, however, the flow characteristics of the MR fluid can be changed from semi-solid to liquid in milliseconds. The damper using MR fluid technology can be regulated efficiently, steplessly, accurately, and reversibly. While at work, vibration converter converts torsional vibration into axial vibration, then MR fluid damper attenuates axial vibration.

For the convenience of discussion, the 3D solid model is built (Fig. 3).

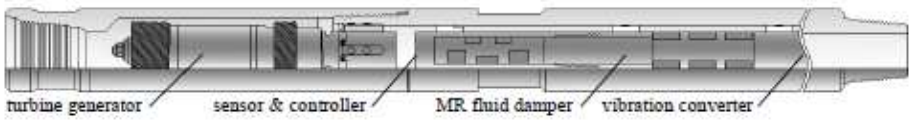

Figure 2: Intelligent damper for drill strings.

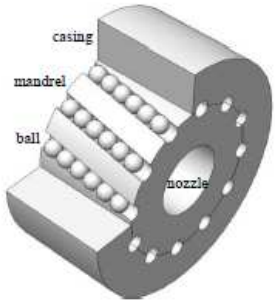

Figure 3: Vibration converter model.

3 Kinematics characteristics analysis of ball

In vibration converter which bears working load, the ball contacts raceway surfaces of mandrel and casing. Whereas a relative movement between mandrel and casing happens, the ball will move along the helicoid. In this case, the trajectory of ball center is a helix as well as the trajectories of the two contact points and passes through the center circle of ball, as shown in Fig. 4. The contact point between ball and raceway surface of mandrel is A and its trajectory is helix l_A, likewise, B and l_B for ball and raceway surface of casing separately, then l for ball center O.

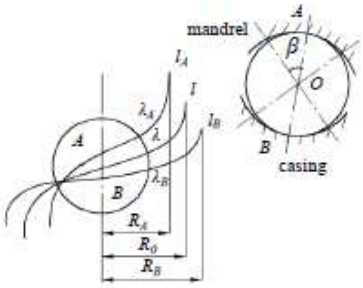

Figure 4: Motion trajectory of ball.

Based on space analytic geometry, suppose the parameter equation of helix l of ball center O [8]:

$$l=\{r_0\cos\theta, r_0\sin\theta, p\theta\}, \tag{3.1}$$

where r_0 is radius of center circle of ball; θ is parameter angle; p is helix parameter; $p=L/2\pi$, L is lead.

Correspondingly, the parameter equation of helix l_A of contact point A is

$$\begin{aligned} l_A=\{&(r_0-r_b\cos\beta)\cos\theta+r_b\sin\lambda\sin\beta\sin\theta,\\ &(r_0-r_b\cos\beta)\sin\theta-r_b\sin\lambda\sin\beta\cos\theta, p\theta+\cos\lambda\sin\beta\}, \end{aligned} \tag{3.2}$$

where r_b is ball's radius; β is contact angle; λ is helix angle.

Similarly, the parameter equation of helix l_B of contact point B is

$$l_B=\big\{(r_0+r_b\cos\beta)\cos\theta+r_b\sin\lambda\sin\beta\sin\theta,\\ (r_0+r_b\cos\beta)\sin\theta-r_b\sin\lambda\sin\beta\cos\theta,p\theta+\cos\lambda\sin\beta\big\}. \tag{3.3}$$

The above formulae are under the condition of right-hand raceway surfaces. As for the left-hand raceway surfaces, take $-p$ instead of p in the formulae. According to the formulae above, the relationships between radii of cylindrical surfaces on which the helices lie R_A, R_B and R_0 (that is radius of center circle of ball r_0),

$$R_A=\sqrt{(r_0-r_b\cos\beta)^2+r_b^2\sin^2\beta\sin^2\lambda},\quad R_B=\sqrt{(r_0+r_b\cos\beta)^2+r_b^2\sin^2\beta\sin^2\lambda}. \tag{3.4}$$

Because the radii of cylindrical surfaces on which the helices l_A, l, l_B lie are different, while at the same lead L, the helix angles λ_A, λ, λ_B differ from each other:

$$\lambda_A=\tan^{-1}\frac{L}{2\pi R_A}=\tan^{-1}\frac{p}{R_A},\quad \lambda=\tan^{-1}\frac{p}{R_0},\quad \lambda_B=\tan^{-1}\frac{p}{R_B}. \tag{3.5}$$

If there exists relative movement between mandrel and casing, ideally, ball center O will move along the helix l with tangential direction of helix l being its velocity direction. The tangent equation can be deduced from Eq. (3.1):

$$-\frac{x-r_0\cos\theta}{\cos\lambda\sin\theta}=\frac{y-r_0\sin\theta}{\cos\lambda\cos\theta}=\frac{z-p\theta}{\sin\lambda}. \tag{3.6}$$

This tangent goes through ball center O $(R_0\cos\theta,R_0\sin\theta,p\theta)$ with its direction number

$$\{l,m,n\}=\{-\cos\lambda\sin\theta,\cos\lambda\cos\theta,\sin\lambda\}. \tag{3.7}$$

In addition, based on Eqs. (3.2)-(3.3), the moving directions of ball in contact points A, B and tangent equations of helices l_A, l_B can be obtained. The direction number, for l_A is

$$\{l,m,n\}=\{-\cos\lambda_A\sin\theta,\cos\lambda_A\cos\theta,\sin\lambda_A\}. \tag{3.8}$$

Also, for l_B:

$$\{l,m,n\}=\{-\cos\lambda_B\sin\theta,\cos\lambda_B\cos\theta,\sin\lambda_B\}. \tag{3.9}$$

The three corresponding tangents of helices l_A, l, l_B are spatial crisscross from each other. By employing space analytic geometry and Eqs. (3.7)-(3.9), the angles γ_{AO}, γ_{BO} between l_A, l_B and tangent of l are obtained:

$$\tan\gamma_{AO}=\frac{d_b\sin\lambda\cos\lambda}{d_0-d_b\cos\beta\cos^2\lambda},\quad \tan\gamma_{BO}=\frac{d_b\sin\lambda\cos\lambda}{d_0+d_b\cos\beta\cos^2\lambda}, \tag{3.10}$$

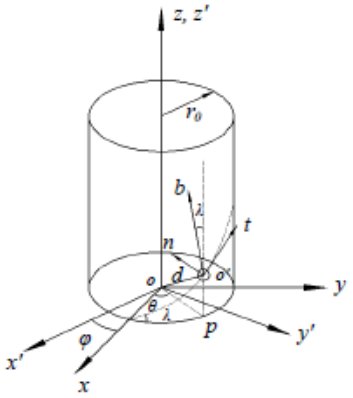

Figure 5: The position of the ball center, o', in the Cartesian coordinates and Frenet coordinate.

where d_0 is diameter of center circle of ball; d_b is diameter of ball.

In the study of kinematics of the vibration converter, three coordinate systems are needed to describe the motion of the ball and its contact behavior. The first (world) coordination system, $ox'y'z'$, is fixed with its z' axis coincident with the axis of mandrel. The second (rotating) coordination system, $oxyz$, also has its z axis coincident with the mandrel axis (Fig. 5), and rotates with the mandrel. The third coordination system, $o'tnb$, is the Frenet frame moving with ball center along the trajectory of ball center. This trajectory, with respect to the frame $oxyz$, is a circular helical line along a circular cylindrical surface with a mean radius r_0, and φ denotes the included angle between the first two coordination systems (Fig. 5).

The coordinate transformation between the first two coordinate systems can be written as

$$x'=x\cos\varphi-y\sin\varphi,\quad y'=x\sin\varphi+y\sin\varphi,\quad z'=z. \tag{3.11}$$

Assuming that a ball has moved an angle θ along the helix angle λ of a mandrel with a lead $d\sin\lambda$, then

$$d\sin\lambda=\frac{\theta L}{2\pi},\quad \tan\lambda=\frac{L}{2\pi r_0}, \tag{3.12}$$

where L is lead; d is the distance between two origins, o and o' (ball center).

The position equation of the ball center, in the rotating coordination system, can be expressed as [9]

$$X=r_0\cos\theta x,\quad Y=r_0\sin\theta y,\quad Z=r_0\theta\tan\lambda z. \tag{3.13}$$

The coordinate transformation between the Frenet frame of ball center and the rotational

coordinate system $oxyz$ can be expressed as

$$x=(-\cos\lambda\sin\theta+\cos\lambda\cos\theta+\sin\lambda)t, \tag{3.14a}$$
$$y=(-\cos\theta-\sin\theta)n, \tag{3.14b}$$
$$z=(\sin\lambda\sin\theta-\sin\lambda\cos\theta+\cos\lambda)b. \tag{3.14c}$$

Now, Eq. (3.13) can be rewritten in terms of the Frenet frame of ball center as

$$X=r_0\sin\lambda\tan\lambda\theta t,\quad Y=-r_0 n,\quad Z=r_0\cos\lambda\tan\lambda\theta b. \tag{3.15}$$

The velocity of ball center, v, can be obtained by differentiating Eq. (3.15) with respect to time:

$$\frac{dX}{dt}=\left(\frac{r_0}{\cos\lambda}\omega_0+r_0\cos\lambda\omega\right)t,\quad \frac{dY}{dt}=0,\quad \frac{dZ}{dt}=-r_0\sin\lambda\omega b, \tag{3.16}$$

where $\omega_0=d\theta/dt$ is the rotational angular velocity, if a ball moving forward in the t-direction along the mandrel surface; $\omega=d\varphi/dt$ is the rotational angular velocity of mandrel.

It will be shown in the next section that the ball can only move relatively to the mandrel in the tangential direction of the Frenet frame of ball canter trajectory, because the ball is confined in the helical groove in direction parallel to the normal plane of the trajectory of ball center. Physically, this means that the contact points between the ball and the mandrel, as well as between the ball and the casing, must be located on this normal plane.

In order to locate these contact points, the contact angle, β, is defined as the angle between the unit normal vector and contact vector. The contact vector is oriented from the ball center toward the contact point, as shown in Fig. 6. Points A, B represent the instantaneous contact points between the ball and the casing and between the ball and the mandrel, respectively, with their contact angles β_A, β_B.

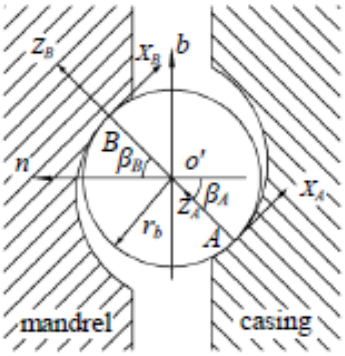

Figure 6: Location of contact points on the normal plane.

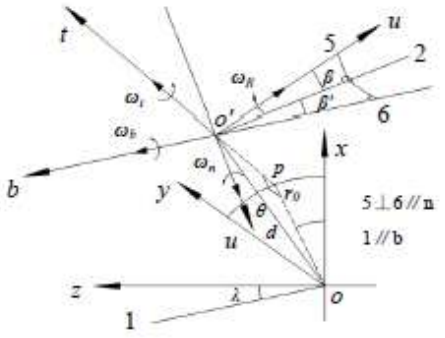

Figure 7: Coordinate system of ball's motion analysis.

We now introduce a pair of new coordinate systems $iX_iY_iZ_i$, with $i=A,B$, between the ball and the raceway such that the X_iY_i plane lies on the plane of contact and Z_i axis lies along the common normal of the two contacting bodies. We also assume point contacts along a diagonal line between the ball and mandrel and casing. The coordinate transformation between the Frenet frame of ball center trajectory and the $iX_iY_iZ_i$ coordinate system is

$$X_i=t,\quad Y_i=(\cos\beta_i-\sin\beta_i)n,\quad Z_i=(\cos\beta_i+\sin\beta_i)b. \tag{3.17}$$

The angular velocity due to ball's spinning is ω_R, the components of ω_R along the t, n, b axis are ω_t, ω_n, ω_b, respectively. The $o'u$ axis is coincident with the spinning axis of a ball, the $o'2$ axis is the projection of the $o'u$ axis in the $o'u$ plane, the angle between the $o'2$ axis and the $o'u$ axis is β, and the angle between the $o'2$ axis and the $-b$ axis is β' [6], as shown in Fig. 7.

It can be seen from Fig. 7, the relationships between ω_t, ω_n, ω_b and ω_R are

$$\omega_t=\omega_R\cos\beta\sin\beta',\quad \omega_n=-\omega_R\sin\beta,\quad \omega_b=-\omega_R\cos\beta\cos\beta'. \tag{3.18}$$

By using Eqs. (3.16)-(3.18), the velocities of contact points A, B on the ball, v_A, v_B, can be achieved

$$\begin{aligned} v_A=&\Big[\frac{r_0}{\cos\lambda}\omega_0+r_0\cos\lambda\omega+r_b(\omega_b\cos\beta_A-\omega_n\sin\beta_A)\Big]tr_b\omega_t\sin\beta_A n\\ &-(r_0\sin\lambda\omega+r_b\omega_t\cos\beta_A)b, \end{aligned} \tag{3.19a}$$

$$\begin{aligned} v_B=&\Big[\frac{r_0}{\cos\lambda}\omega_0+r_0\cos\lambda\omega+r_b(\omega_b\cos\beta_B-\omega_n\sin\beta_B)\Big]t-r_b\omega_t\sin\beta_B n\\ &-(r_0\sin\lambda\omega-r_b\omega_t\cos\beta_B)b. \end{aligned} \tag{3.19b}$$

Therefore, it can be seen from Eq. (3.19) that the velocity of ball has correlation with radius of center circle of ball r_0, helix angle of the mandrel λ, ball's radius r_b and angular velocity of ball's spinning ω_R. Considering the lead $L=\tan\lambda 2\pi r_0$, radius of center circle of ball and helix angle can be bracketed together. Angular velocity of ball's spinning is relevant

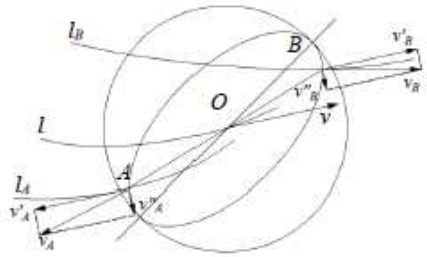

Figure 8: Schematic diagram of ball's motion.

to moment of inertia which depends on ball's radius with a fifth power relationship. So ball's radius is the key factor affecting the velocity of ball.

Suppose the instantaneous velocity of ball center O is v and take ball center O as the instantaneous center of motion, its velocities at contact points A, B are v_A, v_B, as Fig. 8 shows. According to Eq. (3.20) and Fig. 8, v_A, v_B can be decomposed into v'_A, v'_B, which parallel to velocity of ball center, and v''_A, v''_B, which perpendicular to velocity of ball center:

$$v'_A = v_A \cos\gamma_{AO}, \quad v'_B = v_B \cos\gamma_{BO}, \quad v''_A = v_A \sin\gamma_{AO}, \quad v''_B = v_B \sin\gamma_{BO}. \tag{3.20}$$

The space angles formed by v_A, v_B and v are on both sides of the helix l, so the velocity components v''_A, v''_B are in the same direction. Apart from rolling in the tangential direction of the helix l with the linear velocities v'_A, v'_B, there also exists sliding motion perpendicular to line AOB in the raceway, that is the sliding motion on the normal plane. In addition, there still exists spinning round tangent of l. The composite motion of these three types is main motion characteristics of ball in vibration converter.

4 Self-locking effect of vibration converter

In vibration converter, the contact states between mandrel, casing and ball depend on running conditions and stress states. When it is working, the two normal forces acting on ball are non-collinear, due to manufacturing errors of internal and external raceways and ball's sliding. As shown in Fig. 9, the normal forces N_A, N_B acting on contact points A, B are non-collinear when the two contact planes clamping the ball are not parallel and have a included angle 2γ. Under resultant force of N_A and N_B, the ball tends to move toward left, thus generates frictions f_A, f_B at contact points A and B, see Fig. 9. the ball will move left as the resultant force of N_A and N_B is greater than that of f_A and f_B. Alternatively, it will stand still, which is called self-locking effect with the condition of

$$\gamma \leq \tan^{-1}\mu, \tag{4.1}$$

where γ is half of the angle included between the two contact planes; μ is coefficient of sliding friction between ball and plane.

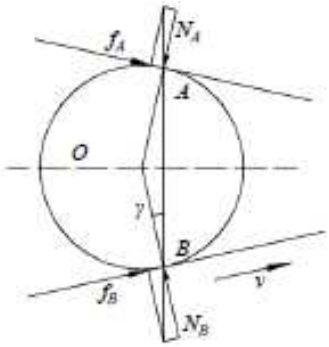

Figure 9: Schematic diagram of self-locking effect.

Under condition of Eq. (4.1), the ball will go right by friction if one of the two planes moves toward the right side. Then it can be clamped much closer between the two planes. With the raise of normal pressure, the friction grows and eventually leads to elastic or plastic deformation of ball and contact planes at the contact points. There exists such kind of motion in the contact areas between ball and raceway in vibration converter, which is called self-locking effect of vibration converter. When ball slides in the normal plane of raceway, it will be pushed into the raceway and produce a reaction force that prevents ball's entrance as a result of self-locking effect. Thus, the friction in vibration converter has a great fluctuation.

5 Contact stress and strain analysis of ball in vibration converter

5.1 Contact states between ball and mandrel, casing

According to hertz contact theory, the elastic contact between ball and raceways as well as mandrel and casing can be considered as elastic contact of two free-form surfaces. The difference lies in principal curvatures in principal planes where the two elastomers contact.

Fig. 10 is schematic diagram of simplified mechanical model of vibration converter, with helix angle λ and contact angle β. Where, A and B are contact points between ball and mandrel and between ball and casing, respectively; R is radius of raceway surface; d_b is ball diameter. Among the principal planes of mandrel which pass through contact point A, one also passes through normal O_1A and axis OO_1, that is the axial section shown in Fig. 11(a). Its radius of principal curvature is R. While the other principal plane passes through axis O_1A and perpendicular to axial section, see Fig. 11(b). Consider helix angle and suppose its radius of principal curvature is R_{22}, then it can be expressed as

$$R_{22}=O_1A/\cos\lambda=(d_0-d_b\cos\beta)/2\cos\beta\cos\lambda. \tag{5.1}$$

As for ball, any secant plane that passes through normal of contact point A can be treated as principal plane of ball and its radius of principal curvature R_{11} and R_{12} equals

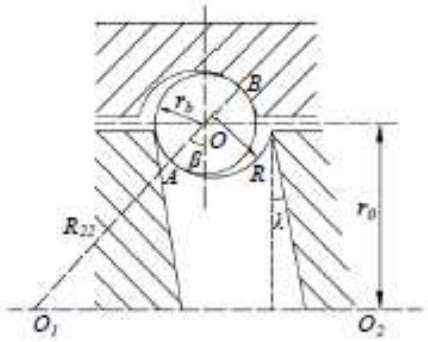

Figure 10: Contact state of vibration converter.

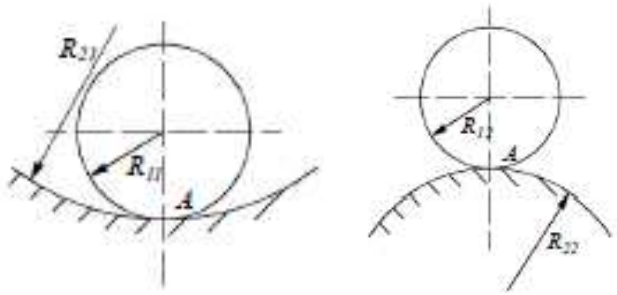

(a) (b)

Figure 11: Principal plane of mandrel (through contact point A).

r_b. Moreover the two principal planes of mandrel can be taken as two principal planes of ball. Principal planes of the two curved surface body are coincident.

The four principal curvatures of ball and raceway of mandrel at contact point A are

$$\rho_{11}=\rho_{12}=\frac{1}{r_b},\quad \rho_{21}=-\frac{1}{R},\quad \rho_{22}=\frac{2\cos\beta\cos\lambda}{(d_0-d_b\cos\beta)}, \tag{5.2}$$

where negative principal curvature denotes concave curve.

Similarly, the two principal curvatures of raceway of casing at contact point B are

$$R_{21}=R,\quad R_{22}=(d_0+d_b\cos\beta)/2\cos\beta\cos\lambda. \tag{5.3}$$

For the same reason, radii of principal curvature of ball at contact point B are $R_{11}=R_{12}=r_b$ and its principal planes coincide with the two principal planes of raceway of casing.

The four principal curvatures of ball and raceway of casing at contact point B are

$$\rho_{11}=\rho_{12}=\frac{1}{r_b},\quad \rho_{21}=-\frac{1}{R},\quad \rho_{22}=\frac{2\cos\beta\cos\lambda}{(d_0+d_b\cos\beta)}. \tag{5.4}$$

5.2 Elastic contact stress and strain of vibration converter

Based on hertz elastic contact theory, when the two free-form surfaces contact under the pressure P, the stress distribution is a semi-ellipsoid on the ellipse contacting surface [8], as shown in Fig. 12.

$$q(x,y)=q_{\max}\sqrt{\left(1-\left(\frac{x}{a}\right)^2-\left(\frac{y}{b}\right)^2\right)}. \tag{5.5}$$

Therefore, total pressure P is the integration $\int_S q(x,y)ds$ of contact stress $q(x,y)$ on the contact area S. From the view of geometry, the integration equals to the volume of the semi-ellipsoid, then

$$P=\frac{2\pi abq_{\max}}{3}. \tag{5.6}$$

Finally, the maximum contact stress

$$q_{\max}=\frac{3P}{2\pi ab}, \tag{5.7}$$

where a and b are major semi-axis and minor semi-axis of contact ellipse, respectively, and can be calculated by

$$a=\alpha\sqrt[3]{\frac{m}{n}P}, \qquad b=\beta\sqrt[3]{\frac{m}{n}P}, \tag{5.8a}$$

$$m=\frac{4}{\rho_{11}+\rho_{12}+\rho_{21}+\rho_{22}}, \qquad n=\frac{8}{3\left[(1-\mu_1^2)/E_1+(1-\mu_2^2)/E_2\right]}. \tag{5.8b}$$

α, β are geometrical factors determined by principal curvatures. E_1, E_2 and μ_1, μ_2 are longitudinal elastic moduli and Poisson's ratio.

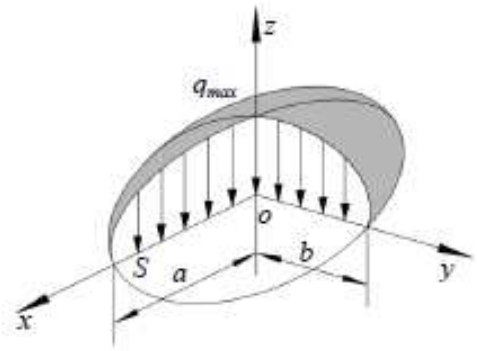

Figure 12: Distribution of contact stress.

Relative displacement of the two contacting elastomers along the z axis, due to elastic compression deformation, is called elastic approach, that is

$$\delta_P = \frac{3P}{2\pi a}\left(\frac{1-\mu_1^2}{E_1}+\frac{1-\mu_2^2}{E_2}\right)J, \tag{5.9}$$

where J is ellipse integration determined by principal curvatures.

If the two elastomers are steel with elastic module $E = 2.1\times10^5$MPa and Poisson's ratio $\mu = 0.3$, it can be rewritten as

$$\delta_P = 8.12\times10^{-7}\times\sqrt[3]{\frac{P^2\sum\rho J}{\alpha}}, \tag{5.10}$$

where $\sum\rho = \rho_{11}+\rho_{12}+\rho_{21}+\rho_{22}$ is called synthetic curvature.

Synthetic curvature of raceway of mandrel is

$$\sum\rho_s = \frac{2}{r_b}-\frac{1}{R}+\frac{2\cos\beta\cos\lambda}{d_0-d_b\cos\beta}. \tag{5.11}$$

Synthetic curvature of raceway of casing is

$$\sum\rho_n = \frac{2}{r_b}-\frac{1}{R}+\frac{2\cos\beta\cos\lambda}{d_0+d_b\cos\beta}. \tag{5.12}$$

Then,

$$\Delta\sum\rho = \sum\rho_s-\sum\rho_n = \frac{4d_b\cos^2\beta\cos\lambda}{d_0^2-d_b^2\cos^2\beta}. \tag{5.13}$$

For the contact points A and B between mandrel and casing, the elastic approaches are different by discrete in the principal curvatures, despite a same contact pressure P. The elastic approach between ball and mandrel is larger than that between ball and casing, which shows the contact stiffness of casing is greater than that of mandrel, and stiffness is inversely related to the increase of helix angle.

6 Case study

In order to simulate the kinematics characteristics of ball accurately, a Computer Aided Engineering (CAE) software is employed to analyze the working mechanical behavior. Because computing time is proportional to the contact element number, possible contact surfaces are pre-estimated according to theory model analysis. Then, a simplified calculation model is set by supposing each ball and the contact states of raceways are identical or at least similar, see Fig. 13 and Table 1. The intelligent damper for drill strings discussed in this paper is suitable for $8-1/2''$ borehole where the casing diameter of vibration converter, inside diameter of casing, outside diameter of mandrel, diameter of nozzle and

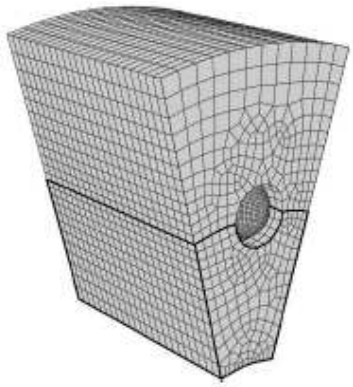

Figure 13: Simplified finite element model.

contact angle of ball and raceway are 172mm, 112mm, 110mm, 51mm, and 40°, respectively. The model built by CAD software is imported into CAE software, when defining the material properties, contact and friction, meshing, finally applying constraints and loadings (that is rotational speed of mandrel $\omega = 15r/min$).

Apply rotational speed to vibration converter to study the effect of ball diameter on the kinematics characteristics of ball. The result can be seen from Fig. 14. The axial velocity of ball decreases gradually and the ball becomes slower and more unstable on its starting with the increase of ball diameter. Particularly, the ball moves reversely and its velocity varies greatly when the ball diameter increases to 15mm.

Apply rotational speed to vibration converter to study the effect of helix angle on the kinematics characteristics of ball. As shown in Fig. 15, the axial velocity of ball decreases with helix angle decreases from 84° to 76°. Notably, self-locking effect of vibration converter discussed above occurs and the axial velocity of ball approaches almost zero when the helix angle is 82°. Therefore, the self-locking effect, besides larger helix angle, should also be taken into consideration when designing the vibration converter.

Now that the effects of ball diameter and helix angle on ball's kinematics characteristics have been studied in above paragraphs, the following will continue in the view of

Table 1: Finite element model.

Material property	Young's modulus	Poisson's ratio	
	210GPa	0.3	
Element type	C3D8R		
Element size	Mandrel	Ball	Casing
	5mm	0.5mm	5mm
Boundary condition	Mandrel	Casing	
	$U1=U2=UR1=UR2=0$	$U1=U2=U3=UR1=UR2=UR3=0$	
Contact type	General contact		
Friction coefficient	Static friction coefficient	Dynamic friction coefficient	
	0.15	0.003	

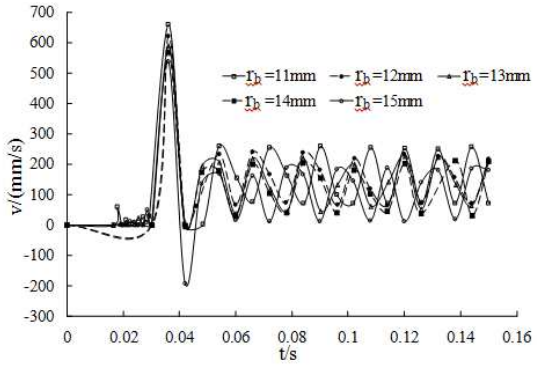

Figure 14: Effect of ball diameter on its kinematics characteristics.

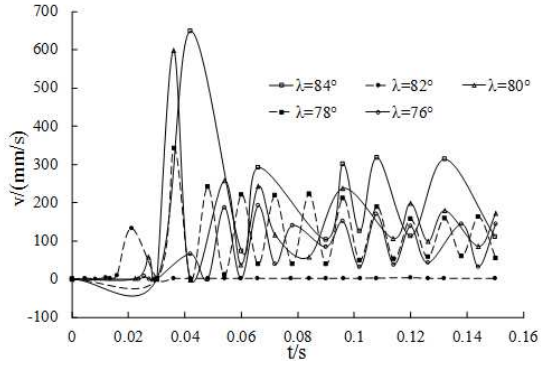

Figure 15: Effect of helix angle on ball's kinematics characteristics.

contact stress. Shown in Fig. 16, while decreasing ball diameter from 15mm to 11mm, the maximum contact stress of ball increases rapidly and fluctuates greatly, which can lead to great possibilities of ball premature failure. This also means kinematics characteristics and contact stress should be comprehensively considered in determining appropriate ball diameter. In addition, a raise in the number of raceways and ball can reduce the contact stress of ball and enhance bearing capacity of vibration converter. Fig. 17 shows the effect of helix angle on contact stress of ball, in which the maximum contact stress of ball decreases with the increase of helix angle. At the helix angle of 80°, the maximum contact stress of ball reaches its minimal value with a relatively lower fluctuation. In this case, the performance of vibration converter can be improved.

7 Conclusions

Taking vibration converter of intelligent damper for drill strings as the study subject and based on Newton's laws of motion, d'alembert's principle, hertz contact theory and world coordinate system, rotating coordinate system, Frenet coordinate system, this paper has deduced kinematics equations of vibration converter, analyzed the influential

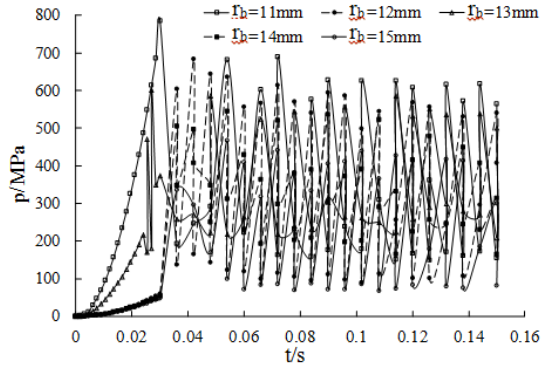

Figure 16: Effect of ball diameter on its contact stress.

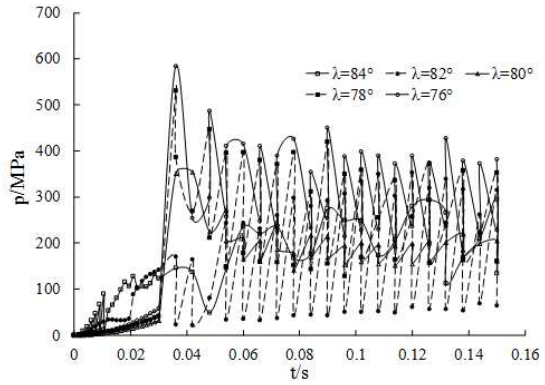

Figure 17: Effect of helix angle on contact stress of ball.

factors of motion state of the ball, established mechanics model of vibration converter, and conducted an explicit dynamics simulation. Altogether, the following conclusions can be drawn:

1. Under the same condition, contact stiffness of casing is greater than that of mandrel, and the contact stiffness of casing diminishes with the increase of helix angle.
2. With the increase of ball diameter, axial velocity of ball decreases gradually and the ball becomes slower and more unstable on its starting.
3. Axial velocity of ball diminishes with the decrease of helix angle. For a better design of vibration converter, the self-locking effect, besides choosing a larger helix angle, should also be considered.
4. With decrease in ball diameter, the maximum contact stress of ball increases rapidly and fluctuates fiercely, which can lead to great possibilities of ball premature failure. Thus, kinematics characteristics and contact stress should be comprehensively considered in determining appropriate ball diameter. In addition, a raise in the number of raceways and ball can reduce the contact stress of ball and enhance bearing ca-

pacity of vibration converter. Maximum contact stress of ball diminishes with the increase of helix angle.

5. The parameters for ball screw of vibration converter in intelligent damper for drill strings $(6-3/4'')$ which often used in $8-1/2''$ borehole drilling are recommended as: 40° for the contact angle between ball and raceway; 80° for the helix angle; 14mm for the width of ball diameter; 112mm for the inside diameter of casing; 110mm for the outside diameter of mandrel; 51mm for the diameter of nozzle.

Acknowledgments

This work was supported by National Natural Science Fund of China (51222406, 51004082), New Century Excellent Talents in University of China (NCET-12-1061), Scientific Research Innovation Team Project of Sichuan Colleges and Universities (12TD007), Sichuan Youth Sci-tech Fund (2011JQ0020), the 7th graduate innovation funds of Southwest Petroleum University (GIFSS0720), and Special thanks to PhD C. S. Shi.

References

[1] M. YAVERI, K. DAMANI AND H. KALBHOR, *Solutions to the down hole vibrations during drilling*, SPE/IADC Drilling Conference, (31 July-7 August 2010), SPE 136956.
[2] M. E. COBERN, C. A. PERRY, J. A. BARBELY, D. E. BURGESS AND M. E. WASSELL, *Drilling tests of an active vibration damper*, SPE/IADC Drilling Conference, (20-22 February 2007), SPE 105400.
[3] X. ZHANG, Study on Structure and Characteristic of Two-Way Shock Absorber, Master's paper, Daqing Petroleum Institute, China, 2007.
[4] D. MUNDO AND H. S. YAN, *Kinematics optimization of ball-screw transmission mechanisms*, Mech. Mach. Theory, 42 (2007), pp. 34–47.
[5] Y. TAKAFUMI, T. YASUYOSHI AND M. SUSUMU, *Study on load distribution and ball motion of ball screw*, J. Japanese Society Tribologists, 48 (2003), pp. 659–666.
[6] X. S. MEI, M. TSUTSUMI, T. TAO AND N. G. SUN, *Study on the load distribution of ball screws with errors*, Mech. Mach. Theory, 38 (2003), pp. 1257–1269.
[7] X. C. SONG, H. K. JIANG, X. R. XU AND Z. Y. ZHANG, *Analysis of elastic deformation for high speed ball screw based on the finite element method*, Journal of Beijing University of Technology, 35 (2009), pp. 582–586.
[8] G. R. CHENG, Design Basic of Ball Screw Transmission, China Machine Press, Beijing, 1987.
[9] M. C. LIN, B. RAVANI AND S. A. VELINSKY, *Kinematics of the ball screw mechanism*, J. Mechanic al Design, 116 (1994), pp. 849–855.
[10] P. A. DU, *Analysis of the elastic contact deformation and rated load of ball straight-rotary pair*, Journal of University of Electronic Science and Technology of China, 23 (1994), pp. 280–285.